



Delft University of Technology

SpiderWeb

Enabling Through-Screen Visible Light Communication

Ye, Hanting; Wang, Qing

DOI

[10.1145/3485730.3485948](https://doi.org/10.1145/3485730.3485948)

Publication date

2021

Document Version

Final published version

Published in

SenSys 2021 - Proceedings of the 2021 19th ACM Conference on Embedded Networked Sensor Systems

Citation (APA)

Ye, H., & Wang, Q. (2021). SpiderWeb: Enabling Through-Screen Visible Light Communication. In *SenSys 2021 - Proceedings of the 2021 19th ACM Conference on Embedded Networked Sensor Systems* (pp. 316-328). (SenSys 2021 - Proceedings of the 2021 19th ACM Conference on Embedded Networked Sensor Systems). ACM. <https://doi.org/10.1145/3485730.3485948>

Important note

To cite this publication, please use the final published version (if applicable).
Please check the document version above.

Copyright

Other than for strictly personal use, it is not permitted to download, forward or distribute the text or part of it, without the consent of the author(s) and/or copyright holder(s), unless the work is under an open content license such as Creative Commons.

Takedown policy

Please contact us and provide details if you believe this document breaches copyrights.
We will remove access to the work immediately and investigate your claim.

SpiderWeb: Enabling Through-Screen Visible Light Communication

Hanting Ye
Delft University of Technology
Delft, The Netherlands
h.ye-1@tudelft.nl

Qing Wang
Delft University of Technology
Delft, The Netherlands
qing.wang@tudelft.nl

ABSTRACT

We are now witnessing a trend of realizing *full-screen* on electronic devices such as smartphones to maximize their screen-to-body ratio for a better user experience. Thus the bezel/narrow-bezel on today's devices to host various line-of-sight sensors would disappear. This trend not only is forcing sensors like the front cameras to be placed *under* the screen of devices, but also will challenge the deployment of the emerging Visible Light Communication (VLC) technology, a paradigm for the next-generation wireless communication.

In this work, we propose the concept of *through-screen VLC* with photosensors placed *under* Organic Light-Emitting Diode (OLED) screen. Though being transparent, an OLED screen greatly attenuates the intensity of passing-through light, degrading the efficiency of intensity-based VLC systems. In this paper, we instead exploit the color domain to build SpiderWeb, a through-screen VLC system. For the first time, we observe that an OLED screen introduces a *color-pulling effect* at photosensors, affecting the decoding of color-based VLC signals. Motivated by this observation and by the structure of spider's web, we design the SWebCSK Color-Shift Keying modulation scheme and a slope-based demodulation method, which can eliminate the color-pulling effect. We prototype SpiderWeb with off-the-shelf hardware and evaluate its performance thoroughly under various scenarios. The results show that compared to existing solutions, our solutions can reduce the bit error rate by two orders of magnitude and can achieve a 3.4× data rate.

CCS CONCEPTS

• Networks → Wireless access networks; Mobile networks.

KEYWORDS

Through-screen VLC, transparent OLED screen, color-pulling effect

ACM Reference Format:

Hanting Ye and Qing Wang. 2021. SpiderWeb: Enabling Through-Screen Visible Light Communication. In *The 19th ACM Conference on Embedded Networked Sensor Systems (SenSys '21)*, November 15–17, 2021, Coimbra, Portugal. ACM, New York, NY, USA, 13 pages. <https://doi.org/10.1145/3485730.3485948>

1 INTRODUCTION

Visible Light Communication (VLC) has been considered as one of the key enablers for future wireless networks such as 6G [9, 32]. In VLC, a transmitter modulates the visible light to send data; a receiver, equipped with photosensors, can detect visible light changes

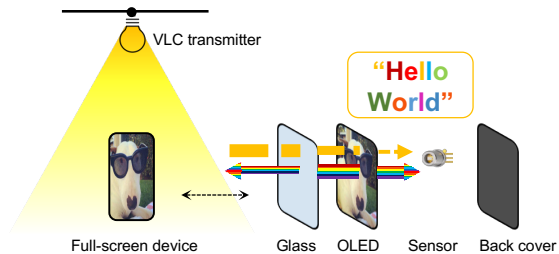


Figure 1: Motivation of this work: there is no space to deploy VLC receivers on the screen of narrow- and no-bezel smartphones. A possible solution could be to deploy VLC receivers under the screen, but the screen will become a 'blocker' and an interferer for the line-of-sight light communication.

and demodulate them into data. VLC has several advantages. For example, the visible light frequency band is about 10000 larger than the RF band. Thus, VLC has the potentials to provide higher-speed wireless communications. Visible light is directional and does not penetrate walls, allowing VLC to achieve high spatial multiplexing.

Because of these advantages, VLC has attracted attention from both academia and industry. It has enabled many promising applications, such as high-speed wireless communication (i.e., Light Fidelity, LiFi) [12], centimeter-level positioning [5, 37, 43], human sensing and gesture recognition [17, 20, 40], vehicular-to-X communication [33, 36], screen/LED-to-camera communication [18, 39, 41], sunlight communication [6, 7, 11, 35], under-water VLC [19], etc. VLC has been deployed in real scenarios. Very recently, pureLiFi announced the first-ever large-scale deployment of LiFi (worth 4.2 million dollars) to provide secure wireless communication [25]. VLC will also be deployed to the Airbus Corporate Jet product line [28].

Although significant progress on research, development, deployment, and standardization of VLC is being witnessed, a direction has been largely neglected by the community: *how to deploy VLC practically on (future) devices, especially on the smartphones that are heavily used by billions of people?* Here, *where* on smartphones to place VLC receivers is ultra important. In state-of-the-art trials of VLC on smartphones, the receivers are mainly deployed on the back and top edge of smartphones, and/or on the smartphone screen [24, 25]. Since VLC access points are usually placed on the ceiling (used for both illumination and communication) and the VLC signal quality is dominated by line-of-sight links, placing VLC receivers onto the front part of smartphones will be beneficial and indispensable. However, the latest trend toward *no-bezel* (i.e., *full-screen*) smartphone designs to increase the screen-to-body ratio [15] brings new challenges to VLC deployment because there will be *no space on the smartphone screen* to place VLC receivers.

In today's most advanced *narrow-bezel* and *no-bezel* smartphones, traditional sensors such as fingerprint sensor, ambient light sensor, and even cameras have been deployed or are being evaluated *under*



This work is licensed under a Creative Commons Attribution International 4.0 License.

SenSys '21, November 15–17, 2021, Coimbra, Portugal
© 2021 Copyright held by the owner/author(s).
ACM ISBN 978-1-4503-9097-2/21/11.
<https://doi.org/10.1145/3485730.3485948>

the screen [3, 22]. Motivated by this existing technical evolution on smartphones, in this paper, we ask the following question: *is it possible to also place visible light sensors under the screen to create through-screen VLC systems, as depicted in Figure 1?* If this exciting objective can be achieved, we can boost VLC deployment on future smartphones because it does not sacrifice their full-screen designs.

Although through-screen VLC looks promising, the screen in-between the VLC transmitter and the receiver might seriously degrade the system performance because the screen could become a blocker. For example, an LCD screen is not transparent and blocks light, and thus, a photosensor placed under an LCD screen will not detect any light from the transmitter! Thanks to technological advances in the screen area, now most smartphones have replaced LCD screens with Organic LED (OLED) screens. This is because an OLED screen is thinner, lighter in weight, more efficient in illumination, and more importantly, better at displaying contents. An OLED screen could also be made *transparent*, allowing light to pass through. This is one of the key enablers for through-screen VLC.

However, after the incident light passes through the glass of an OLED screen, the light intensity is still sharply reduced. Moreover, the modulated light signals are seriously interfered with by the light emitted from the screen when the screen is on. At the same time, the VLC sensor is closer to the screen than to the VLC transmitter. As a result, at the receiver, the intensity of the light emitted by the screen is often several orders of magnitude of the intensity of the modulated light from the transmitter. Without perfect synchronization between the transmitter and the screen, it would be difficult to demodulate intensity-based VLC signals.

For this reason, we exploit the color domain to realize through-screen VLC. Compared with intensity-based modulations such as On-Off-Keying (OOK), color-based modulations such as Color-Shift-Keying (CSK) only care about the chromaticity of visible light and is not sensitive to the light intensity. However, it is challenging to realize reliable CSK-based VLC because the screen content dynamically changes, interfering with the CSK signals. If we adopt the CSK constellation points specified in the IEEE 802.15.7 VLC standard [1], these points will be severely offset. Therefore, the first challenge on designing a through-screen VLC system is *how to decode the signal that has been interfered by the screen light*. In particular, the screen color changes dynamically when displaying different contents.

In this work, we observe from measurements that the received CSK constellation points shift toward the screen color point after being interfered by the screen, as illustrated in Figure 2. The positions of the received symbols are distributed between the transmitted CSK symbol constellation points and the detected screen color point. That is, the transmitted CSK symbols are *pulled* to the screen color point. We refer it as *color-pulling effect* introduced by the screen on the CSK signals. Motivated by the observation that the received symbols form lines from the CSK symbol constellation points to the screen color point, we propose to use a slope-based demodulation method to distinguish the received symbols. It works well for the CSK with low modulation levels, such as 4-CSK.

Although the slope-based demodulation algorithm can reduce the Bit Error Rate (BER) in CSK-enabled through-screen VLC, we encounter the second challenge: *with higher-level CSK modulations specified in the IEEE 802.15.7 standard (e.g., 8-CSK and 16-CSK) and under many screen colors, the slope-based demodulation alone cannot*

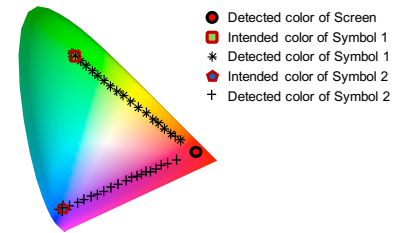


Figure 2: The color-pulling effect caused by the transparent OLED screen at the photosensor of the VLC receiver.

distinguish the received constellation points. In higher-level CSK modulations such as 8-CSK and 16-CSK, some of the lines (caused by the color-pulling effect) that connect their constellation points with the screen color point could *overlap* with each other, making the demodulation of these constellation points almost impossible.

To tackle this challenge, we design a new color-based modulation scheme named SpiderWeb Color-Shift Keying (SWebCSK). The design is motivated by the structure of spiderweb. We set the detected screen color at the sensor as the hub of the spiderweb, and search for the suitable constellation points from each ray of the spiderweb. We maximize not only the Euclidean distances among constellation points, but also maximize the minimal angle between any two lines caused by the color-pulling effect. This design ensures that the lines will not overlap with each other, benefiting the demodulation of received color-modulated symbols at the receiver.

We have also tackled other challenges related to the practical design and implementation of a through-screen VLC system. When generating CSK/SWebCSK signals at the transmitter, a linear current drive could be leveraged. However, the normalized radiant power of the tri-color RGB LEDs versus the DC drive current is not linear, additionally considerable hardware overhead and complexity will be introduced. In this work, we use three high-frequency PWM signals to control each channel of the tri-color LED and we identify the formulation to calculate the duty circles of each PWM signal, considering the power/non-flickering constraint and the attenuation of visible light in the air as well as when the light passes across the OLED screen. We also solve at the receiver an over-saturation problem that is specific in through-screen VLC.

We successfully prototype the proposed system using off-the-shelf hardware. Combining all the design components, we successfully enable through-screen VLC under different screen colors and different screen brightness. The proposed SWebCSK modulation and the slope-based demodulation could achieve very low BER in different scenarios. Below we summarize our main contributions:

- We propose the concept of through-screen VLC and validate its feasibility by prototyping with off-the-shelf devices.
- We observe a color-pulling effect of transparent OLED screens on color-based CSK signals. This effect greatly degrades the BER performance of through-screen VLC systems.
- We design a color-based and spiderweb-inspired SWebCSK modulation scheme. Together with our proposed slope-based demodulation, we can improve the BER performance greatly under different screen color and brightness.
- We thoroughly evaluate the performance of our system in different scenarios. The results demonstrate that compared to existing solutions, our methods can reduce the BER by two orders of magnitude and achieve a 3.4× data rate.

2 BACKGROUND

2.1 Types of Screen

There are currently two main types of screen: Liquid Crystal Display (LCD) and OLED. Below we briefly introduce them.

LCD screen. It has three main components: backlight panel, liquid crystal, and two polarizing plates called Polarizer and Analyzer, as illustrated in Figure 3(a). The liquid crystal does not emit light; thus, a backlight panel is needed (except in reflective displays) as a light source to illuminate the display panel. The liquid crystal layer can change the polarization direction of incident light when applied different voltages, thereby controlling the light/dark states of the screen. This feature has been used for passive VLC [6, 7, 33, 36].

OLED screen. It also has a sandwich structure. The difference is an OLED screen does not need a backlight panel, and the thick liquid crystal layer is replaced by a thin organic emissive layer wrapped by the anode and cathode, as shown in Figure 3(b). Thus, an OLED screen is thinner than an LCD screen. To display content, the anode of OLED is built with transparent materials and covered with glass. An OLED screen is self-luminous. The cathode can also be built with transparent electrode materials such as transparent indium tin oxide to form a *transparent screen*.

2.2 Screen Refresh Rate & Brightness Control

The refresh rate is an important screen parameter that determines the quality of the screen. The screen refresh rate of common devices such as smartphones, monitors, and TVs, is 60 Hz. Some high-end monitors have supported a refresh rate of 144 Hz. In recent years, the refresh rate of smartphone screens is being increased to 90 Hz and 120 Hz. For any screens, the content displayed on the screen remains unchanged between two consecutive screen refreshes.

There are two ways to control the brightness of a screen. One is Direct Current (DC) dimming, which changes circuit current to control the power of the emitted light. The other one is Pulse-Width Modulation (PWM) dimming that changes the number of ON and OFF states of the screen in a unit time to have various brightness, as shown in Figure 4. PWM dimming is widely used in OLED screens.

2.3 Standard Color Space

A popular color space chromaticity diagram is CIE 1931 [8],¹ which mimicks human perception of color. *The diagram maps all colors perceivable by human eyes to two chromaticity parameters - x and y - as shown in Figure 5, where the monochromatic light with different wavelengths forms the line on the periphery of the horseshoe shape.* Each screen might have a different color display range. The RGB color spaces used in most commercial screens are shown in Figure 5. The sRGB and DCI-P3 color gamuts are widely used in devices; the Adobe RGB color gamut is mostly used in professional photography.

2.4 Color-Shift Keying Modulation

The Color-Shift Keying (CSK) modulation scheme was proposed in the IEEE 802.15.7 standard for VLC [1]. CSK exploits the design of LED luminaires which use three separate (Red, Green, and Blue) LEDs to generate white light. With three LEDs channels R/G/B, such luminaires can be configured to provide a variety of colors using the mixture of Red (R), Green (G), and Blue (B). CSK modulates the

¹CIE is the French abbreviation for the International Commission on Illumination.

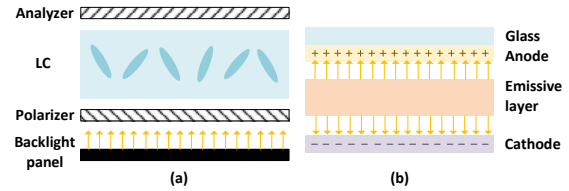


Figure 3: Simplified diagrams of screens: (a) LCD; (b) OLED. An OLED screen is thinner and lighter than an LCD screen.

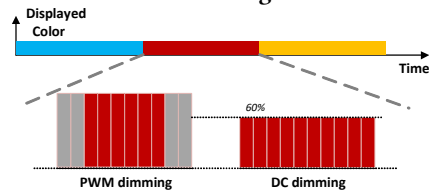


Figure 4: OLED screen refresh rate and brightness control.

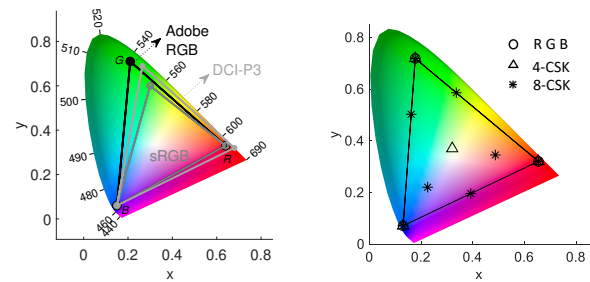


Figure 5: CIE color space.

Figure 6: CSK modulation.

signal by modifying the output power combinations of the three colors. Since different devices use different RGB color spaces, we need a standard color space to unify color standards. Depending on the operating frequency of the red, green, and blue LEDs of the source, a *modulation triangle* is formed within the standard color space, as indicated in Figure 6. Regardless of whether the screen uses sRGB or Adobe RGB, most of its color space is included in the modulation triangle of this work. The constellation symbols are chosen inside the triangle. In addition, given the RGB coordinates of the modulation triangle,² the CSK constellation points, as shown in Figure 6, can be directly calculated from the specification in [1].

3 SPIDERWEB COLOR-SHIFT KEYING

In this section, we first introduce our observation of OLED screen's impact on traditional CSK signals. Then, we present SpiderWeb CSK (SWebCSK), a key scheme we design to enable through-screen VLC.

3.1 Screen's Color-Pulling Effect on CSK Signal

Intensity-based modulations (e.g., OOK [34], Pulse Position Modulation (PPM), and Pulse Amplitude Modulation (PAM) [42]) are widely used in VLC systems. In through-screen VLC, visible light is greatly attenuated when it passes through the screen because the transparency of OLED screens is still not high [16]. This discourages the use of intensity-based modulations in through-screen VLC. Also, since at the receiver the detected screen light intensity is usually much higher than the attenuated modulated visible light, it will be difficult to eliminate the interference of the dynamic screen light

²In IEEE 802.15.7, IJK is used to represent the variable apex coordinates of the modulation triangle. For simplification in this work, I is represented as the red coordinate point R , J as the green coordinate point G , and K as the blue coordinate point B .



Figure 7: 4-CSK.

Figure 8: The time domain illustration of the screen's color-pulling effect on the CSK signals.

on intensity-based VLC signals.³ Compared with intensity-based modulations, the demodulation of color-based CSK signals does not depend on the signal strength, but exploits the position of the detected CSK signals mapped in the CIE color space. Equipped with a true color sensor, the VLC receiver can directly read the X, Y, and Z values of detected CSK signals, which are the imaginary three primary colors after the R, G, and B transformations to meet the CIE 1931 standard chromaticity observer function. The transformation of coordinates from X, Y, and Z values to the CIE 1931 space is

$$x = X / (X + Y + Z), \quad y = Y / (X + Y + Z). \quad (1)$$

When the visible light passes through the color filter of a color sensor, a portion of the photons is filtered out. To collect enough photons, a common color sensor needs to wait for a certain amount of time, known as the integration time or the conversion time (cf. the datasheet of the sensor TCS34725 for example [4]). Therefore, what we receive through the color sensor is not an “instantaneous” CSK signal but an *integral* signal. As introduced in Section 2.2, due to the simplicity of hardware, PWM dimming is usually adopted by OLED screens for brightness control. To avoid flickering, the PWM controlling signal has a much higher rate than the screen refresh rate. Thus even when the color displayed on the screen does not change between two screen refreshing actions, the state of an OLED screen actually switches very fast between ON and OFF. In through-screen VLC, the color sensor (photosensor) is placed under the screen. Therefore, the color sensor integrates not only the transmitted CSK signal but also the ‘random’ light emitted by the screen. In practice, it could be impossible to cancel the screen light because the ON/OFF state of the screen and the transmitted CSK signals cannot be practically synchronized.

3.1.1 Color-pulling effect. We use two illustration figures to show this effect. The transmitter sends the 4-CSK symbols calculated according to [1]. The transparent OLED screen is placed between the transmitter and the receiver, and the color sensor of the receiver is deployed under the screen. The experimental color gamut results are shown in Figure 7. We could observe a phenomenon in which the detected CSK signals at the color sensor are always on the line segment connecting the sending symbol point and the screen color point.⁴ We denote the CSK symbol for the green light as A, and the CSK symbol for the red light as B. As shown in Figure 7, when symbol B is transmitted and the screen color is red, the reception of symbol B is not affected. Nevertheless, when symbol A is transmitted and the screen color is red (corresponding symbol B), we

³Simple intensity-based modulations such as OOK can still work in through-screen VLC. We will discuss the fusion of color-based and intensity-based modulations for through-screen VLC in Section 7.

⁴Most modern devices, such as smartphones, use professional programs to calibrate their screen color to the standard color spaces as introduced in Section 2.3. Thus, we do not need additional calibration procedures to get the accurate screen color coordinates.

come with a line segment from A to B, where the starting point of the line segment is symbol A, and the endpoint is close to B. This means that when the screen is illuminated, the original symbol A (when the screen is not illuminated) is pulled closer to the symbol B. We call this phenomenon as the *color-pulling effect* of the screen on CSK signals, which pulls the originally sent CSK symbol points to the color point of the screen.

From the time-domain’s perspective, we assume that the transmitter sends symbol A and symbol B successively within 8 time slots (the length of each time slot is equal to the integration time of the color sensor). Figure 8 shows the color signal receiving process, which contains the color symbols sent by the transmitter, the color displayed on the screen,⁵ and the color detected at the under-screen sensor. Because the transmitter does not know the specific period of the screen signal, the transmitted signal and the screen signal are not synchronized. In addition, the screen adopts PWM dimming. In other words, the screen is ON within a certain period of time, and is OFF in another period of time. Also, the frequency of PWM is much lower than transmitted signal frequency. As shown in Figure 8, in the first two time slots, the symbols sent are wholly disturbed by the screen, so the original green symbol point of the sensor output is pulled to the orange symbol point. In the third time slot, a jump occurred in the middle of the screen, changing from the original red light to no light, and thus the sending symbol A is only disturbed by part of the red light of the screen. Therefore, the symbol points collected by the sensor in the third time slot are yellow symbol points. The transmitter starts to send the red symbol point B from the 5th time slot. Because the screen is transparent or red at this time, from the 5th to the 8th time slot, the output of the sensor in the receiver is still at the red symbol point. That is, the red symbol point A is not affected when the screen color is red. The above analysis in the time domain explains in principle the occurrence of screen’s color-pulling effect on the CSK signals.

3.1.2 Impact of the screen brightness. The distribution of the points on the line connecting the constellation point and the screen color point depends on the screen brightness. Interestingly, when the screen brightness increases, more points are shifted from the original constellation point to distribute on the line. This can be observed from our measurements shown in Figure 9(a). The result in Figure 9(b) is to analyze the distribution of constellation points under different screen brightness. When the screen is OFF, there is no interference from the screen color. Thus, the sampled points are distributed around the original constellation points. When the screen is fully ON, there is already interference from the screen, and thus, the received points are nearly distributed around the screen color. When the screen is ON but its brightness is less than 100%, the points are distributed on the line as well as the constellation and screen color points. Also, we calculate the normalized distance between interfered point and constellation point with respect to the distance between the constellation point and the screen color point.

3.1.3 Is a slope-based demodulation method enough for tackling the color-pulling effect on CSK signals? Since the points are distributed on the lines, we could not use the traditional method to

⁵The screen usually displays a multi-pixel image so that the overall screen shows a variety of colors. However, the sensor has a small sensing area under the screen. Thus, we assume that the screen color perceived by the sensor is the color of a pixel.

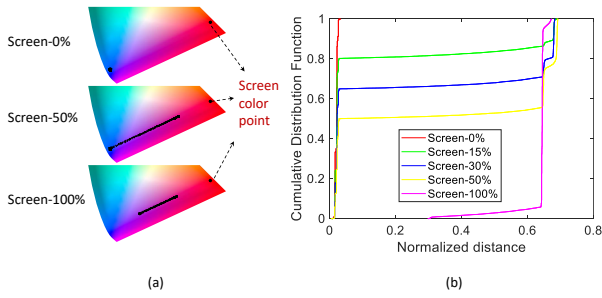


Figure 9: Color-pulling effect vs. screen brightness.

demodulate the received data. But this line has motivated us to design a slope-based scheme to demodulate the received signals. The color-pulling effect from the screen inspires us not only to use the distance between each constellation point in the CIE 1931 space to demodulate by implementing minimum Euclidean distance detection, but also to use the slope from each constellation point to the screen color point for demodulation, that is, use the angular space of CIE 1931 space. This *only* works with low-level CSK modulation under certain screen colors such as the 4-CSK under the red displayed on the screen as shown in Figure 7, where the slopes are different. However, when the screen color is yellow-green, the slopes of the blue symbol point and the white symbol point of 4-CSK are overlapped. Especially, in CSK with higher modulation levels such as 8-CSK under red screen as shown in Figure 10, there are more possibilities for multiple CSK symbols to overlap with each other, which is completely indistinguishable. Therefore, we need to redesign the distribution of the constellation points.

3.2 SWebCSK Overview

In our proposed SWebCSK modulation, we also exploit the different combinations of R/G/B colors to modulate data. Different from the traditional CSK where the constellation points in the constellation diagram are fixed for a certain modulation level, in SWebCSK, the constellation points are optimized dynamically based on the current screen color detected at the photosensor of the VLC receiver. By doing this, we could significantly alleviate the color-pulling effect caused by the screen and thus can enable through-screen VLC.

Defining the line connecting the current screen color point and an SWebCSK constellation point as a *ray*. To ensure the through-screen VLC signals has a low bit error rate, we should maximize the distances between the constellation points. Due to the color-pulling effect of the screen, we should also separate the rays as much as possible. Based on these intuitions, we have the following designing principles for M -SWebCSK, where M is the modulation level:

- (1) The minimum Euclidean distances among the M constellation points should be as large as possible;
- (2) The rays should be separated from each other to the largest extent. In particular, two rays should not overlap with each other (recall the issue in 8-CSK, cf. Figure 10).⁶

Although we can form an optimization problem to find the constellation points, the complexity is usually high because the problem

⁶An exception is when the screen color point falls in between two constellation points.

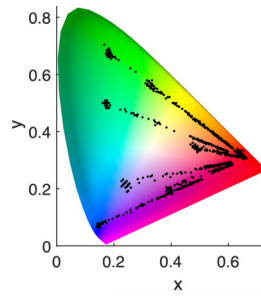


Figure 10: 8-CSK.

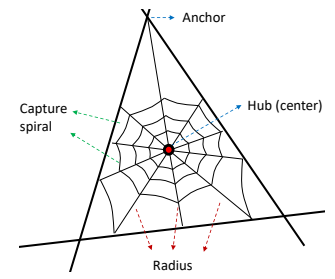


Figure 11: Structure of a spiderweb.

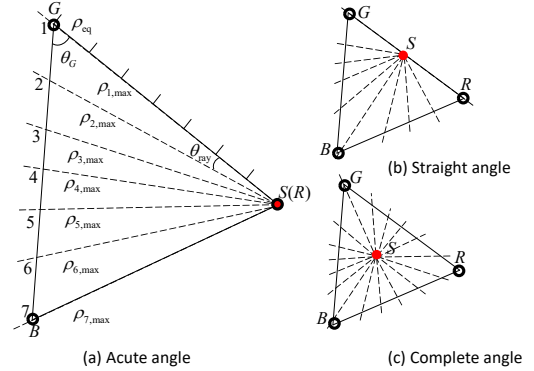


Figure 12: Model and modulation angle.

would be non-conductive and non-convex [23]. To reduce the complexity, in this work we instead propose a heuristic to obtain the proper SWebCSK constellation points. Next we present the details.

3.3 SWebCSK Constellation Design

Our solution is motivated in part by the structure of the spiderweb. In a spiderweb as shown in Figure 11, *hub/center* is a place for the spider to rest; *radius* is composed of non-sticky lines for the spider to crawl on; *capture spiral* is built with sticky silk for catching insects. The constellation design in SWebCSK is to select the most suitable intersections of the capture spiral and the radius to meet with the two design principles presented in Section 3.2.

Before introduce the details, we first make the following definitions. For the triangle that confines the modulation space, we define the three apexes as $R \triangleq (x_R, y_R)$ (Red), $G \triangleq (x_G, y_G)$ (Green), $B \triangleq (x_B, y_B)$ (Blue). These points are fixed. We define the screen color at a time slot as $S \triangleq (x_S, y_S)$. This point changes based on the color displayed on the screen. For the M -SWebCSK, we need to find M constellation points in the modulation space. Denote the designed CSK constellation points as $u_i \triangleq (x_i, y_i), \forall i \in \{1, \dots, M\}$.

Motivated by how a spider weaves its web, in our algorithm, we first establish a spiderweb-alike framework within the modulation space. This framework will give us the list of potential constellation points. Then we use a greedy algorithm to choose the optimal constellation points for our SWebCSK. Without the loss of generality and for explanation simplicity, we assume the screen is displaying Red color. That is, S and R overlap with each other in the constellation space, as illustrated in Figure 12(a). We also use this figure to explain our proposed algorithm. The algorithm consists of three steps:

Step 1) Establish the spiderweb-alike framework. To build such a framework, we first need to find a primary constellation point,

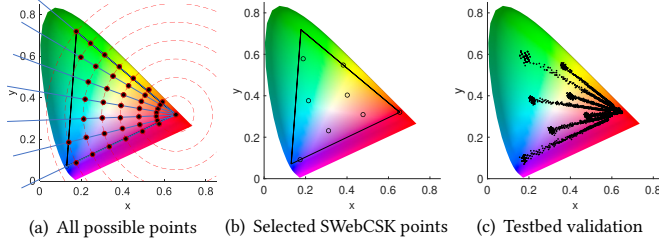


Figure 13: SWebCSK constellation design ($M = 8$).

which is similar to the hub or centre of a spiderweb where the spider rests. Since the candidate constellation point that overlaps with the screen color point is least affected by the color-pulling effect of the screen, we use this one as the primary constellation point. We number it as the M -th constellation point, that is, $u_M = (x_S, y_S)$.

Once we identify the hub constellation point, we calculate the modulation angle θ . This angle determines how many rays can we embed into the modulation space, i.e., affecting the modulation level of our proposed SWebCSK. The larger the modulation angle θ , the higher M will be. A higher M means more bits can be transmitted in the unit time/symbol. But note that with a specific modulation angle, a higher M usually leads to higher BER. For the modulation angle, there are only three cases: 1) *Acute angle*, when the screen color point overlaps with one of the vertexes of the modulation space; 2) *Straight angle* ($\theta = 180^\circ$), when the screen color point falls on the edges of the modulation space (excluding the three vertexes); 3) *Complete angle* ($\theta = 360^\circ$), when the screen color point is within the triangle. These three cases are illustrated in Figure 12.

To meet with the second requirement (cf. Section 3.2), the minimum angle can be maximized by evenly splitting the modulation angle θ . Therefore, the screen coordinates can be the origin, and each ray equally divides the modulation angle. Note that to eliminate the color-pulling effect, only a point on each ray can be selected as a constellation point in the proposed SWebCSK to guarantee that there is a minimum angle θ_{eq} between any two constellation points and the screen color point. In addition to the point u_M , we still need $(M - 1)$ rays to extract another $(M - 1)$ constellation points. When θ is an acute angle or a straight angle as shown in Figure 12(a) and (b), we need $(M - 1)$ rays to form $(M - 2)$ angles; when θ is a complete angle, $(M - 1)$ rays form $(M - 1)$ angles. Denoting θ_{ray} as the angle between each two neighboring rays, we have

$$\theta_{ray} = \begin{cases} \theta/(M - 2), & \text{if } \theta \leq 180^\circ \\ \theta/(M - 1), & \text{if } \theta = 360^\circ \end{cases} \quad (2)$$

Therefore, if the screen color point S is on the three edges of the modulation triangle, then 180 degrees could be leveraged to split the $(M - 1)$ rays, and thus, a higher level of SWebCSK could be formed. Furthermore, if the screen color point S is within the modulation triangle, 360 degrees can be used, and the level of the SWebCSK could be further improved. In summary, the current screen color has a significant impact on the levels of SWebCSK we would form.

After obtaining the rays, we continue to find the suitable constellation points on each ray. Again, we follow the building process of a spiderweb. In the framework with the $(M - 1)$ rays, we draw concentric circles to connect the rays, all centered around the primary constellation point (screen color point). The maximum radius of the circle that has an intersection with the modulation triangle

Algorithm 1 Select constellation points from the candidate sets

Input: $\mathcal{A} = \{\rho_M\}$

$C_i, i \in \mathcal{B} \triangleq \{1, \dots, M - 1\}$

Output: \mathcal{A}

- 1: Set the screen color point as a constellation point u_M
 - 2: **while** $\mathcal{B}! = \emptyset$ **do**
 - 3: Select the ray j with the least number of candidate points:

$$j = \arg \min_{i \in \mathcal{B}} C_i$$
 - 4: Use the max-min metric to select the point on the j th ray.
 - 5: $\mathcal{A} \leftarrow \mathcal{A} \cup \rho_j$
 - 6: $\mathcal{B} \leftarrow \mathcal{B} / j$
 - 7: **end while**
-

is $\rho_{max} \triangleq \max\{d_{SR}, d_{SG}, d_{SB}\}$. Let K denote the number of circles. The larger the K , the more potential constellation points we will have. For simplicity, we assume the inter-circle distance is fixed and denoted by ρ_{eq} . Then we have $\rho_{eq} = \frac{\rho_{max}}{K-1}$. The intersection of each ray and each circle can be a candidate CSK constellation point for CSK on that ray. According to the law of sines, the maximum length of the i -th ray within the modulation triangle can be calculated as⁷

$$\rho_{i,max} = d_{SG} \frac{\sin \theta_G}{\sin(\theta_G + (i - 1)\theta_{ray})}, \forall i \in \{1, \dots, M - 1\}. \quad (3)$$

The number of candidate constellation points that can be placed on each ray is computed as $C_i = \left\lfloor \frac{\rho_{i,max}}{\rho_{eq}} \right\rfloor + 1, \forall i \in \{1, \dots, M - 1\}$. As a result, the set of available constellation points in the modulation triangle area is obtained. All the candidate CSK constellation points and the constructed spiderweb are shown in Figure 13(a).

Step 2) Select constellation points from the candidate sets. In Step 1, we have already selected the screen color point as the primary constellation point. For $u_M, \rho_M = 0$. We then put point u_M into the set \mathcal{A} , which is the set to store the selected SWebCSK constellation points. To select the remaining $M - 1$ points, we use the ‘‘ray-point’’ procedure. We first identify on which ray to select the constellation point, then find the best constellation point on that ray. The constellation points should be picked from the ray with the smallest number of candidate constellation points first. Therefore, the index of the starting ray is selected as $j = \arg \min_{i \in \{1, \dots, M-1\}} C_i$. Then we use the Max-min metric to select a point from the j th ray as a constellation point. The Max-min metric maximizes the minimum distance between the currently selected point and the previous points in set \mathcal{A} . According to the law of cosines, the Max-min metric can be expressed as follows:

$$n = \arg \max_{n \in C_j} \min_{m \in \mathcal{A}} \sqrt{\rho_m^2 + \rho_n^2 - 2\rho_m \rho_n \cos(\theta_{mn})}, \quad (4)$$

where $C_j \triangleq \{1, \dots, C_j\}$. Also, the distance from the selected constellation point on the j -th ray to the screen color point S is as $\rho_j = (n - 1)\rho_{eq}$.

We repeat the above procedure until we find all the M constellation points. The whole procedure is shown in Algorithm 1.

Step 3) Convert the constellation points from polar coordinates to xy coordinates. The SWebCSK constellation points obtained from

⁷Here we only give the result when θ is an acute angle. The expression of $\rho_{i,max}$ when θ is straight/complete angle is omitted due to the space limitation.

Step 2 are expressed in the polar coordinate with the screen color point S as the origin. They need to be further transformed into the xy coordinates in the CIE 1931 coordinate system. When the modulation angle θ is an acute angle, the conversion from the polar coordinates to the xy coordinates can be done as follows:

$$x_i = \tilde{\rho}_i \cos \tilde{\theta}_i, \quad y_i = \tilde{\rho}_i \sin \tilde{\theta}_i, \quad (5)$$

where $\tilde{\rho}_i = \sqrt{\rho_i^2 + \tilde{\rho}_S^2 - 2\rho_i\tilde{\rho}_S \cos \lambda_i}$, $\lambda_i \triangleq \arctan \left| \frac{y_S - y_G}{x_S - x_G} \right| - \theta_{\text{ray}}(i-1) + \arctan(y_S/x_S)$, $\tilde{\rho}_S \triangleq \sqrt{x_S^2 + y_S^2}$, and $\tilde{\theta}_i$ is expressed as

$$\tilde{\theta}_i = \begin{cases} \arctan \frac{y_S}{x_S} + \arccos \frac{\tilde{\rho}_i^2 + \tilde{\rho}_S^2 - \rho_i^2}{2\tilde{\rho}_i\tilde{\rho}_S}, & \lambda \geq 0, \text{ or } \lambda < -\pi \\ \arctan \frac{y_S}{x_S} - \arccos \frac{\tilde{\rho}_i^2 + \tilde{\rho}_S^2 - \rho_i^2}{2\tilde{\rho}_i\tilde{\rho}_S}, & -\pi \leq \lambda < 0 \end{cases}. \quad (6)$$

3.3.1 Preliminary validation. We use the designed 8-SWebCSK constellation points as shown in Figure 13(b) at the transmitter. We place the color sensor under the red screen to detect the transmitted CSK signals. The received constellation points are shown in Figure 13(c). It can be seen that due to the influence of the color-pulling effect, each constellation point of 8-SWebCSK shifts to the red screen point to form seven non-overlapping line segments. The end points of the seven lines formed simultaneously do not overlap with the origin of the red screen, which also helps detect the eighth CSK constellation point at the origin of the screen.

4 SYSTEM DESIGN

We consider a through-screen VLC with a transmitter and a receiver, as illustrated in Figure 1. The transmitter is equipped with an RGB LED and a driver circuit. The visible light emitted from the LED is modulated in the color domain to transmit data wirelessly. At the receiver, we use a true color sensor that can directly output the X , Y , and Z values of the detected light. We consider an OLED screen at the receiver. The color sensor is placed under the OLED screen, similar to the front camera and ambient light sensor placed in the most advanced smartphones [3, 22]. The screen color detected by the color sensor of the receiver is shared with the transmitter. Next, we present the design details of the transmitter and the receiver.

4.1 Transmitter Design

The block diagram of the VLC transmitter is shown in Figure 14. We use three PWM signals to separately control the R/G/B channels of the LED to generate different colors. The controller generates three high-frequency PWM signals with different duty cycles through internal timers to control the average output power of the RGB LED, thereby generating different colors. Although the linear variable current driver has been used to generate different driving current for producing different colors, it often requires the polynomial fitting of more than third order to obtain the normalized optical power of different color [23]. Leveraging PWM signals can avoid tackling the non-linearity of LEDs. The circuit is also simple, easy to implement, and compatible with existing transmitter infrastructures.

Generating the SWebCSK signals. The transmitter receives the binary data and codes them by assigning designed SWebCSK constellation points in the CIE-1931 space. In order to reduce the bit error rate of the system, SWebCSK symbols are coded by gray code

from symbol 1 to symbol M . According to the current color of the screen, the transmitter calculates SWebCSK constellation points based on the method presented in the last section. For a given color constellation point, we need to know the output optical power of R, G, B LED. In order to avoid flickering, the output optical power of R, G, B LED should satisfy $P_R + P_G + P_B = 1$. Suppose that, given a RGB LED in transmitter, a desired output chromaticity of (x_m, y_m) is required (the constellation point coordinates are obtained using the three steps presented in Section 3.3). Substitute the measured x_p and y_p , $p \in \{R, G, B\}$, the output optical power P_R , P_G and P_B required for RGB light can be calculated as

$$\begin{bmatrix} P_R \\ P_G \\ P_B \end{bmatrix} = \begin{bmatrix} x_R & x_G & x_B \\ y_R & y_G & y_B \\ 1 & 1 & 1 \end{bmatrix}^{-1} \begin{bmatrix} x_m \\ y_m \\ 1 \end{bmatrix}, \quad (7)$$

where x_m and y_m are the coordinates of the m th constellation point. Note that in the system, we do not need to calculate the inverse of the matrix in (7). When the LED in the transmitter is fixed, x_p and y_p , $p \in \{R, G, B\}$ are all known to the transmitter, and the inverse of the entire matrix can be calculated in advance. However, we are still unable to realize accurate CSK constellation point coordinates in the transmitter based on P_R , P_G and P_B . For example, if we realize the white point in the CIE 1931 diagram, the output power of the corresponding R, G, and B LEDs should all be 33.3%. In fact, if the PWM duty cycle is configured to (33%, 33%, 33%), the light emitted by the transmitter is not real white light. This is because the luminous efficiency of different colors of light is different. Therefore, we need to know the luminous efficiency of the RGB LEDs.

Since Y represents Luminosity in the CIEXYZ space, we have tried to use Y to simulate the result of the change in the PWM signal duty cycle. However, the actual performance is abysmal, and the modulation of any CSK constellation point cannot be achieved. Nevertheless, by consulting the datasheet of the true color sensor, X channel detects visible light with a wavelength of 600 nm, which is close to the red wavelength range. Similarly, Y channel can detect green light with a wavelength of 555 nm, and Z channel can detect blue light with a wavelength of 445 nm. Therefore, we use the X , Y , and Z channels to calculate the input red, green and blue light irradiance regarding the photodiode's area within the conversion time interval (E_e), which is expressed as $E_e = \frac{\text{FSR}_{E_e}}{N_{\text{CLK}}} \text{MRES}$, where FSR_{E_e} is the full-scale range of detectable input light irradiance E_e , in $\mu\text{W}/\text{cm}^3$ (can be found in [2]); N_{CLK} denotes the number of clock cycles within the predefined conversion time interval; MRES is the digital output value of the conversion (X, Y, Z).

Figure 15 shows the measured input light irradiance regarding the photodiode's area within the conversion time interval versus different duty cycle signals and the corresponding fitted RGB three-color power response. It can be seen that the red/green light has the lowest/highest luminous efficiency. Thus, we set the maximum luminous power of red light as the total emission power of the emitter, and η_R^{max} , η_G^{max} , η_B^{max} in the figure represent the achievable R, G, B maximum duty cycle when total emission power is reached.

Therefore, after substituting the required CSK symbol coordinates, we can get the normalized RGB LED radiation power from (7). Finally, the duty cycle of the PWM signal that controls the RGB LED is calculated as: $\text{PWM}_p = P_p \eta_p^{\text{max}}$, $p \in \{R, G, B\}$.

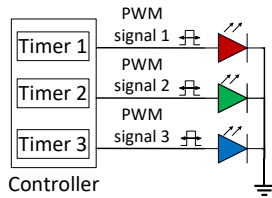


Figure 14: Circuit diagram of the transmitter.

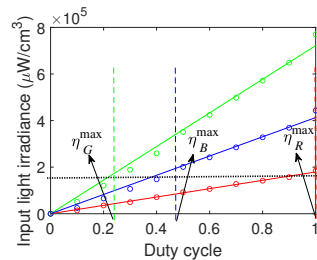


Figure 15: Electro-optical response of the RGB LED.

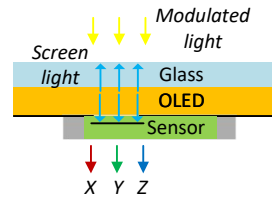


Figure 16: Diagram of the receiver hardware.

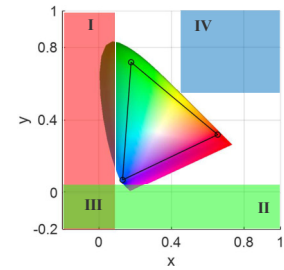


Figure 17: Diagram of over-saturation recovery area.

Channel precompensation. There are two types of visible light attenuation in the system: 1) the attenuation of visible light propagating in the air, and 2) the attenuation of visible light when it passes through the screen medium, known as the Glass Attenuation Factor. Different colors of light have different attenuation under these two attenuation situations. Also, the attenuation faced by different colors of light depends on the distance. In this work, we regard these two types of attenuation as the attenuation of the CSK symbol in the communication channel. In RF communication, the transmitted signal is usually pre-coded to resist channel fading. Similarly, three dynamic compensation factors can be added in transmitter of the SpiderWeb system to compensate for the lower light level at the receiver according to varying distance. The calibrated duty cycle signal of the RGB LED is $\overline{PWM}_p = PWM_p + c_p$, $p \in \{R, G, B\}$.

To complete the channel compensation, the transmitter periodically sends a pilot, which contains a flag and three symbols of R, G, and B light in a sequence. After receiving the flag, the receiver calculates c_R , c_G , c_B , respectively, and then feeds them back to the transmitter. The transmitter will use this calibration factor until the next channel calibration. Since the pilot is sent out periodically, the transmitter can quickly adapt to changing channel condition to make receiver can detect accurate CSK constellation point.

4.2 Receiver Design

As shown in Figure 16, the receiver is composed of a transparent OLED screen and a true color sensor, and the sensor is placed directly under the screen where it emits light. The sensor outputs the X, Y, Z from three channels after detecting the light. The X, Y, and Z channel data streams received by the receiver first pass through the first module to perform over-saturation detection and restore abnormal points. Then through energy detection, the received signal is divided into the part interfered by the screen color signal and the part not interfered by the screen color signal. Next, we use different demodulation methods to demodulate different parts of the received signal. Finally, we detect the preamble of the demodulated signal, find the starting point of the data, and map received symbols to the data bit stream.

4.2.1 Over-saturation recovery. Since the sensor is placed directly under the screen, the light intensity value emitted by the screen that the sensor can receive is extremely high. Because the ADC output accuracy range of the sensor is n bits and sometimes the external light intensity is too strong, the sensor at the receiver is in over-saturation, resulting in abnormal points in the received CSK symbol. Although we can eliminate this kind of over-saturation

by reducing the gain of the sensor, it will also greatly reduce the performance of the system because the light intensity emitted by the screen is much higher than the light intensity of the received signal. Fortunately, we find that the occurrence of over-saturation points often caused one or more of the X, Y, and Z channels of the output signal to recourt from 0. As a result, points not located in the modulation triangle or points are not located in the CIE 1931 chromaticity diagram. Therefore, for the occasional saturation abnormal point, the specific position of the point in the figure is used to compensate. We denote the over-saturation state of the three channels of X, Y, and Z as \hat{X} , \hat{Y} , and \hat{Z} respectively. As shown in Figure 17, the abnormal points are all in areas I to IV. When the abnormal constellation point is in area I, the x coordinate of the abnormal constellation point is very small at this time. It may be that only the X channel is over-saturated, or both X and G channel are over-saturated. It can be denoted as $\{\hat{X}\}$ and $\{\hat{X}, \hat{Z}\}$. When the abnormal constellation point is in area I, the y coordinate is extremely small. At this time, the saturation is $\{\hat{Y}\}$ or $\{\hat{Y}, \hat{Z}\}$. When the abnormal constellation point is in area III, the saturation situation is $\{\hat{X}, \hat{Y}\}$ or $\{\hat{X}, \hat{Y}, \hat{Z}\}$. Finally, since the saturation of the Z channel will increase the x and y coordinates, the abnormal constellation point saturation corresponding to area IV is $\{\hat{Z}\}$.

It can be found that the G channel may be saturated from regions I to III. Therefore, we follow the sequence of I+III, II, IV to detect abnormal points and compensate X, Y, Z channel, respectively. Each compensation value is the ADC maximum output value $2^n - 1$. Abnormal over-saturation points can then be restored to the normal CSK symbol points.

4.2.2 Demodulation. Since CSK signals are all normalized maximum power, although the channel attenuation for different colors of light is different, power compensation is performed. Nevertheless, the signal power received at the receiving end remains at a constant level. Moreover, because the screen is closer to the sensor at the receiver, the light intensity of the different colors of light emitted by the screen received by the sensor is much higher than the modulated light signal after screen attenuation, far exceeding one to two orders of magnitude. Therefore, the threshold can be set according to the average power of the modulated light at the transmitter + screen OFF signal points, and modulated signal at the transmitter + screen ON signal points.

For modulated signal at the transmitter + screen OFF signal point, we calculate ΔE [30] to measure the difference between the colors of two pixels in CIExyZ color space. ΔE is the Euclidean distance

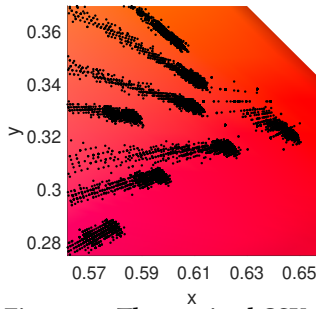


Figure 18: The received CSK signal cluster.

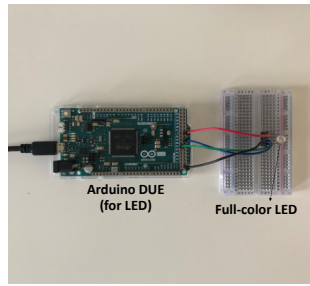


Figure 19: Our implemented SpiderWeb transmitter.

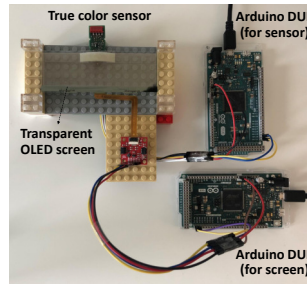


Figure 20: Our implemented SpiderWeb receiver.

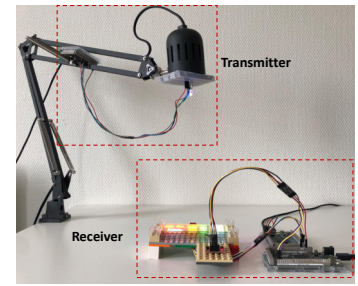


Figure 21: The basic experimental setup.

between two colors in the x, y -plane of the CIEyZ space. We select the smallest ΔE to match the color of a symbol to designed colors by SpiderWeb algorithm (cf. Section 3.3). The received sampling point is denoted as $r_i \triangleq (x_i^r, y_i^r)$, and the SWebCSK constellation coordinates are denoted as $u_j \in \mathcal{M} \triangleq \{1, \dots, M\}$. The optimal minimum distance decoder can be expressed as $u_i^* = \arg \min_{u_j \in \mathcal{M}} \|r_i - u_j\|_2$, where u_i^* is the decoded symbol.

The modulated signals at the transmitter + screen ON signal points are usually clustered together, as shown in Figure 18. If we simply recover the required signal through slope detection, when the signal point interfered by the screen signal is very close to the screen color signal point, the coordinates will swing slightly affected by the noise. It will have a greater impact on slope detection. Therefore, in this part, we again divide the slope detection into two parts: for the first part when the transmitted signal is most affected by the screen color and when it is located in a smaller modulation triangle compressed after the superimposition of the screen signal, we still use the minimum Euclidean distance detection; for the other part that is outside the smaller modulation triangle, we use the minimum slope detection. The optimal slope decoder can be expressed as $s_i^* = \arg \min_{s_j \in \mathcal{M}} \left(\left| \frac{y_i^r - y_S}{x_i^r - x_S} - \frac{y_j - y_S}{x_j - x_S} \right| + \left| \frac{|y_i^r - y_S|}{x_i^r - x_S} - \frac{|y_j - y_S|}{x_j - x_S} \right| \right)$, if $d_i > d_{th}$; otherwise, $s_i^* = \arg \min_{\bar{s}_j \in \bar{\mathcal{M}}} \|r_i - \bar{u}_j\|_2$, where $\bar{s}_j \in \bar{\mathcal{M}}$ is the set of CSK symbol points that are fully interfered by the screen, d_{th} is the predefined threshold, and $d_i \triangleq \|r_i - u_M\|_2$ is the distance between received sampling point and screen color point.

4.2.3 Preamble detection. To decode data from the received signal, we first need to detect the preamble of the frame. In VLC, the preamble is designed and used for frame detection and synchronization [27]. The pattern of preamble is usually fixed with a total of $2K$ alternating ONs and OFFs (i.e., $2K$ ON-OFF patterns). For example, the OpenVLC platform adopts 24 alternating ONs and OFFs as the preamble [10, 34]. However, due to potential screen signal interference, it is impossible to confirm whether the pilots that send all CSK symbols can be successfully decoded and demodulated, and confirm the correct starting position of the data symbol. Thus we send several CSK symbols of the same color on the screen as pilots.

5 IMPLEMENTATION

Transmitter. A snapshot of our implemented SpiderWeb transmitter is given in Figure 19. We use an off-the-shelf full-color LED (Kingbright WP154A4SEJ3VBDZGC [14]) in the transmitter front-end. The peak wavelengths of R, G, B light of this LED are 640 nm,

461 nm, and 515 nm, respectively. The measured color coordinates (x, y) associated with this RGB LED are $(x_R = 0.6544, y_R = 0.3205)$, $(x_G = 0.1776, y_G = 0.7188)$, and $(x_B = 0.1307, y_B = 0.0711)$. An Arduino DUE, a low-cost and open-hardware embedded development platform with an 84 MHz processor, is used as the processing unit at the transmitter. We leverage three independent PWM ports of the Arduino DUE to control the RGB LED separately for generating various colors. The frequency of the PWM signals is set to 1 MHz.

OLED screen. We use the transparent OLED screen Sparkfun LCD-15079 [31] in our prototype.⁸ The colors supported at different pixels of this screen are fixed, and a large part of the screen is just transparent and cannot display any colors. From the rest of this screen, we identify three parts that can display different colors and are large enough to cover our photosensor when the photosensor is placed under that part: red (0.6544, 0.3205), yellow-green (0.44, 0.5), and white (0.3350, 0.3722). The OLED screen is controlled by a dedicated Arduino DUE. The control range of the screen brightness is from 0 to 31, where 0 corresponds to no light on the screen, and 31 corresponds to a duty cycle of 100% for the PWM control signal of the screen, and the screen brightness is the highest.

Receiver. The prototype of the VLC receiver is shown Figure 20. We use the true color sensor AMS AS73211 [2], controlled by an Arduino DUE, to detect the color-based VLC signals. The response of AS73211 conforms to the CIE 1931 standard. Its maximum internal clock frequency is 8.2 MHz, and the maximum supported I2C clock frequency is 400 kHz. Under the maximum clock frequency, the adjustable gain range of AS73211 is $\{1x, 4x, 16x, 64x, 256x\}$, and the sampling integration time is from 125 μs to 2048 ms. In our implementation, we set the gain to 64x and the sampling integration time to 125 μs .⁹ The sensed data is transmitted through a serial port to a laptop for processing, which has an Intel i7 CPU and 32 GB memory. The proposed signal processing and the slope-based demodulation are implemented in Matlab.

6 PERFORMANCE EVALUATION

In this section, we present the evaluation of SpiderWeb in different scenarios. We use Bit Error Rate (BER) and (normalized) data rate as the metrics. The default experimental setup is shown in Figure 21.

⁸Although its name has “LCD”, it is indeed an OLED screen as specified in [31].

⁹A very short integration time of the color sensor will lead to the detection failure of the modulated signals; however, with a very long integration time, the color sensor will be over-saturated. Similar results apply to the gain setting of the color sensor. In our implementation, we use the minimum sampling integration time, together with the color sensor gain of 64x, to obtain the highest data sampling rate and under these settings, we can still detect the modulated visible light signals after screen attenuation.

Table 1: Comparison under different screen colors ($M = 4$)

Screen color	d_{min}		θ_{min} (rad)	
	4-CSK	4-SWebCSK	4-CSK	4-SWebCSK
Red	0.3372	0.2330	0.4942	0.5702
Yellow-green	0.3372	0.1763	0	1.5708
White	0.3372	0.2538	1.9896	2.0944

Table 2: Comparison under different screen colors ($M = 8$)

Screen color	d_{min}		θ_{min} (rad)	
	8-CSK	8-SWebCSK	8-CSK	8-SWebCSK
Red	0.1934	0.1209	0	0.1901
Yellow-green	0.1934	0.1220	0	0.5236
White	0.1934	0.1416	0	0.8976

Table 3: 8-SWebCSK constellation points (under red screen)

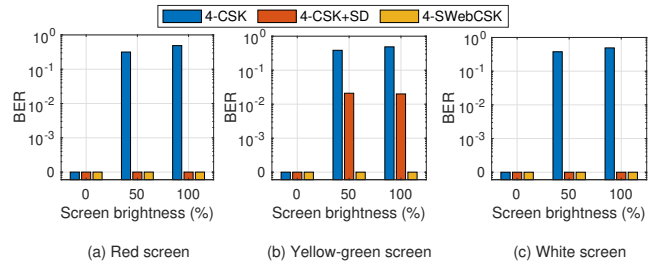
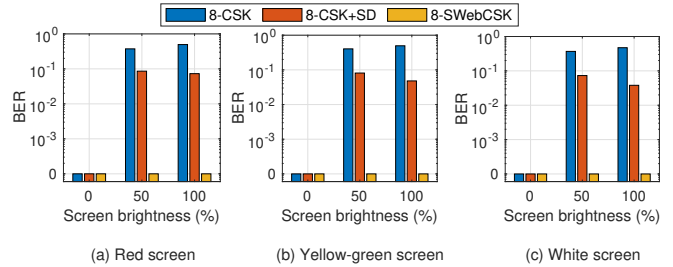
Gray code	Constellation coordinates	(PWM_R, PWM_G, PWM_B)
000	(0.3819, 0.5481)	(43, 60, 0)
001	(0.1886, 0.5785)	(4, 42, 9)
011	(0.4013, 0.4032)	(49, 35, 16)
010	(0.2141, 0.3762)	(12, 42, 22)
110	(0.4773, 0.3091)	(65, 15, 18)
111	(0.3108, 0.2312)	(33, 16, 27)
101	(0.1736, 0.0915)	(8, 0, 42)
100	(0.6544, 0.3205)	(100, 0, 0)

6.1 SWebCSK vs. CSK

Before we present the evaluations of SpiderWeb, we first compare the performance of SWebCSK with that of traditional CSK.

Constellation. We compare our SWebCSK constellation design with the traditional CSK design specified in the IEEE 802.15.7 standard [1]. The results for $M = 4$ and $M = 8$ are shown in Table 1 and Table 2, respectively. The minimum distance among the 4-CSK and 8-CSK constellation points in the IEEE standard is always larger than the minimum distance under our 4-SWebCSK and 8-SWebCSK. However, in the angle space formed by the screen color point on the CIE 1931 diagram, the angle between different constellation points of 8-CSK to screen color point (i.e., the rays; cf. Section 3.2) overlap. For 4-CSK, when the screen color is yellow-green, the angles from the two constellation points to the screen also overlap. In our 4-SWebCSK and 8-SWebCSK, we not only optimize the minimum angle between different rays, but also adapt the optimal constellations based on the detected screen color. Thus, the minimum angles (important in through-screen VLC) among 4-SWebCSK and 8-SWebCSK constellations are higher than those of 4-CSK and 8-CSK. Due to space limitations, we only list the constellation points of 8-SWebCSK, as shown in Table 3. It also gives the corresponding PWM duty cycles to achieve these constellation points.

BER. In this experiment, three brightness of the screen are considered: 0%, 50%, and 100%. we place the transmitter and the receiver at a distance of 10 cm. For the traditional CSK modulated signals, we consider two demodulation methods: 1) use the minimum Euclidean distance to distinguish different symbols; 2) use proposed slope-based demodulation (CSK+SD) method, cf. Section 4.2.2. For our SWebCSK modulated signals, we use our slope-based demodulation. For the modulation level $M = 4$ and $M = 8$, the BER results

**Figure 22: BER under different screen colors when $M = 4$.****Figure 23: BER under different screen colors when $M = 8$.**

are shown in Figure 22 and Figure 23, respectively. We can observe that the BER of 4-CSK and 8-CSK detected by the minimum Euclidean distance are close to 0.5 when the screen is lit up. Under this BER, data transmission is not possible. Using our slope-based detection, 4-CSK reduces the BER to 0 when the screen colors are red and white; when the screen color is yellow-green, under which the angles from the two CSK symbol points to the screen color point overlap, the BER is still below 10^{-1} , showing the advantage of our proposed slope-based demodulation. In 8-CSK, the angles from several constellation points to the screen color point overlap with each other. Thus the BER falls below 10^{-1} . For our designed 4-SWebCSK and 8-SWebCSK, the BER is lower than 10^{-3} regardless of the screen color and the screen brightness, demonstrating that SWebCSK is a key enabler for through-screen VLC.

Normalized data rate. We also evaluate the data rate obtained from traditional CSK and our SWebCSK. For M -CSK, a CSK symbol represents $\log_2 M$ bits. With a larger M , the transmitter can send more bits in a unit time slot. However, a larger M often leads to a higher BER. The achievable data rate of 4-CSK, 8-CSK and our 4-SWebCSK and 8-SWebCSK changes with different color and brightness. Figure 24 shows the normalized data rate averaged over different scenarios (i.e., different screen color: red, yellow-green, and white; and 3 different screen brightness: 0%, 50%, and 100%). We can observe that system data rate is increased by at least 300%. This means SWebCSK can carry more data than the traditional CSK under dynamic screen color and brightness changes. We can observe that when the modulation level $M = 4$, our SWebCSK can improve the data rate by 200%. When $M = 16$, the data rate of CSK is almost zero because the BER is too high; while 16-SWebCSK achieves 5 \times data rate when normalized to that of the 4-CSK. On average, our proposed SWebCSK could achieve 3.4 \times data rate when compared to the traditional CSK.

6.2 SpiderWeb Evaluation

Now we evaluate the system performance of SpiderWeb.

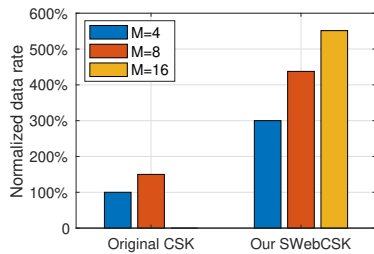


Figure 24: Data rate vs. schemes.

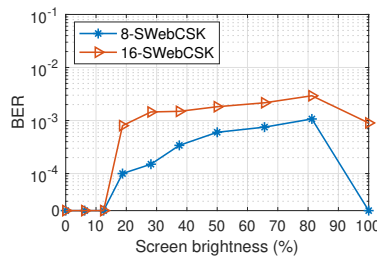


Figure 25: BER result vs. brightness.

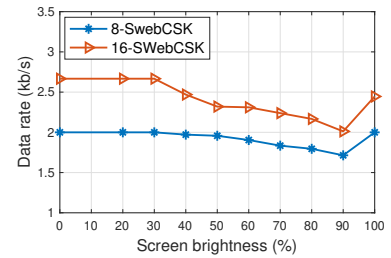


Figure 26: Data rate vs. brightness.

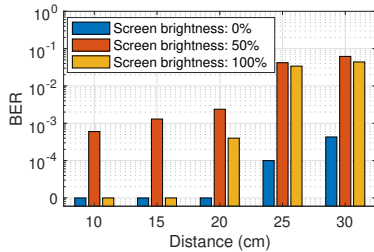


Figure 27: BER result vs. distance.

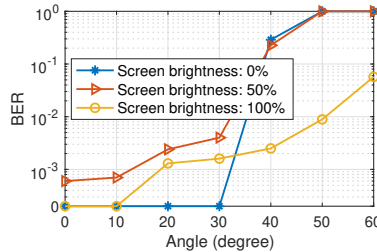


Figure 28: BER result vs. angle.

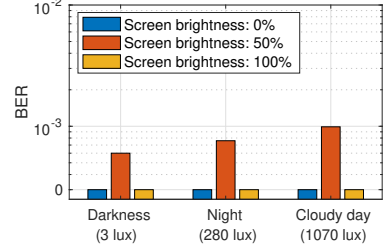


Figure 29: BER result vs. ambient light.

Impact of screen brightness. The brightness of the transparent OLED screen determines how much the transmitted signal is interfered by the screen. Usually, the brighter of the screen, the more transmitted symbols are interfered. When the screen brightness is 100%, all the signals are interfered by the screen. The experimental BER under different screen brightness are shown in Figure 25. Here, 16-SWebCSK is evaluated under the screen color of yellow-green. Overall, the BERs of 8-SWebCSK and 16-SWebCSK are below 10^{-3} and below 10^{-2} , respectively. We observe that with both 8-SWebCSK and 16-SWebCSK, in general, the BER gradually increases with a brighter screen. An exception is that when the screen is fully lit, the BER of 8-SWebCSK is 0 and the BER of 16-SWebCSK reduces to 10^{-3} . The main reason is that the screen signal and the transmitted VLC signals are not synchronized. Since the screen brightness is not constant, with energy detection, we cannot perfectly distinguish all the VLC signals that have been interfered by the screen from those that have not, which brings inevitable misjudgments when the screen is ON but not fully lit. When the screen is fully lit, it is easy to get a priori information that all the received VLC signals are interfered by the screen. Thus, the slope-based SWebCSK detection can still achieve a significantly low BER.

We also measure the achievable data rate of SpiderWeb under different screen brightness, as shown in Figure 26. For 8-SWebCSK, the data rate is between 1.7 kb/s and 2 kb/s; for 16-SWebCSK, the data rate changes from 2 kb/s and 2.6 kb/s. The current bottleneck is the slow response of the low-cost color sensor. The achievable data rate could be significantly improved with advanced color sensors.

Impact of distance. Next, we evaluate the system performance when the transmitter is placed at different distances from the screen/receiver. Here, we use the maximum gain 256x of the sensor to maximize the communication distance. Because the channel attenuation of RGB light is different, the corresponding CSK constellation point correction is performed at the transmitter end for each distance. The BER results are shown in Figure 27. With an OFF screen, the BER is lower than 10^{-3} at a distance of 30 cm. When the screen

brightness reaches 50% and 100%, the BER at the distance of 20 cm is still lower than 10^{-2} .

Impact of angle. We also evaluate the performance of SpiderWeb when the receiver is placed in different directions to the transmitter. We fix the distance between the transmitter and screen to 10 cm and vary the relative angle between them. The results are shown in Figure 28. We can see that the BER performance decreases severely when the angle between the transmitter and the receiver exceeds 30° . On the other hand, the BER performance is still better when the screen is fully lit, although the angle exceeds 30° . At an angle of 50° , the BER is close to 10^{-2} . The reason behind could be that when the angle is large, the intensity of the CSK signals detected by the sensor under the screen is minimal and does not exceed its output threshold, resulting in a sharp increase in the BER when the screen brightness is OFF. However, if the screen is fully lit, the intensity of the CSK signal detected by the sensor exceeds its output threshold after adding the screen light, thereby can report the detection value. In other words, when the angle is large, the screen light could help the signal detection in SpiderWeb.

Impact of the ambient light conditions. Lastly, we study the impact of different ambient light conditions on the system performance. Three different ambient light conditions are considered: (1) Darkness (average light intensity: 3 lux); (2) Night with indoor illumination (average light intensity: 280 lux); (3) Cloudy day (average light intensity: 1070 lux). The impact of the ambient light level on the BER is shown in Figure 29. When the screen is OFF and fully bright, the BER is 0 under all the three conditions. With a screen brightness of 50%, the BER in all three conditions is still lower than 10^{-3} . It is worth noting that due to our over-saturation recovery method (cf. Section 4.2.1), even in the presence of ambient light, our system can still achieve a BER of 0 when the screen is fully bright.

7 LIMITATIONS AND DISCUSSIONS

Low data rate. The highest data rate we can achieve in the current SpiderWeb is about 2.6 kb/s, though it is about 3.4× compared to

that of the traditional CSK. The main bottleneck is the low speed of the color sensor. The minimum sampling time of the color sensor is 125 μ s (we have configured the color sensor to its fastest speed mode). We also use oversampling to remove the sampling points affected by inter-symbol interference. These factors limit the data rate of SpiderWeb. With a faster color sensor or a camera, and faster signal processing methods, we could break the rate bottleneck at the receiver. Besides, when the screen color is with the modulation triangle area (with a modulation angle of 360°) we could further increase the modulation level, such as to 32-SWebCSK or even 64-SWebCSK, to further improve the data rate of the system. Another method is to combine CSK with the Intensity Modulation (IM) [42]. Through the sensor fusion of a photodiode and a color sensor, a joint IM-CSK modulation scheme could be designed to further increase the system data rate of through-screen VLC.

Short communication distance. Currently, the communication distance of SpiderWeb is short. This is because the used RGB LED is low power (its maximum electric power dissipation can only reach 120 mW). Higher-power RGB LEDs used for normal indoor illumination can be leveraged to improve the communication distance. The different luminous efficiency of R/G/B channels of the LED is another main reason for the low light emission power. To avoid flickering, the power envelope of the CSK symbols is fixed. Due to the barrel effect, the transmission power of the CSK symbol is based on the highest optical output power of the lowest luminous efficiency color. LEDs with a higher visible light output power of the R color could increase the communication distance.

Fully dynamic OLED screen. Currently, we build and evaluate SpiderWeb with a transparent OLED screen that displays different colors at different pixels. We manually move the screen to various locations to change its displayed color to evaluate the proposed through-screen VLC. This is because we could not buy a transparent OLED screen from the market whose colors can be changed dynamically in the software. Our proposed solutions for through-screen VLC could work under such a dynamic screen because the refresh rate of a screen is usually about 60 Hz, which is much lower than the symbol rate (several kHz) in our current implementation. The screen refresh interval can be interpreted as channel coherence time. The transmitter could know the current screen color in two ways: 1) the transmitter detects the screen color directly; 2) the receiver detects the screen color and sends the information to the transmitter through an uplink channel. Based on the color of the screen, the transmitter and the receiver can establish new SWebCSK constellations for the data transmission.

Multiple transmitters. When there are multiple transmitters sending data concurrently, the received CSK symbol at the single-pixel color sensor could be the superposition of the CSK symbols from multiple transmitters, causing interference. Without any particular design at the transceivers, the system performance could be degraded significantly. A possible solution is to exploit under-screen multi-pixel camera at the receiver to overcome the interference from multiple transmitters. Under-screen cameras are being adopted in today's advanced full-screen smartphones such as ZTE AXON30 and Xiaomi MIX4. Note that a single transmitter can also use multiple RGB LEDs to transmit more data; with a under-screen multi-pixel camera at the receiver to form a multiple-input and multiple-output link, the system data rate could be increased.

8 RELATED WORK

CSK modulation in VLC. It has been adopted in the IEEE 802.15.7 VLC standard [1] and studied in [13, 21, 23]. The authors in [23] optimize the CSK constellations to improve the system performance. In [21], the authors design a light-to-frequency converter as a CSK receiver to avoid using ADC, leading to a low-cost VLC system. CSK is also used in LED-to-camera communication system to increase the data rate [13]. These studies mainly optimize and utilize CSK-based VLC with different receivers. In our SpiderWeb, we consider a more challenging and very promising scenario where the screen at VLC receivers could “block” and interfere with the communication with visible light. We observe the color-pulling effect and propose the SWebCSK modulation scheme to solve it. Accordingly, we can enable through-screen VLC with extremely low bit error rate, which cannot be achieved by the above state-of-the-art studies.

Sensing with under-screen line-of-sight sensors. The trend toward *narrow-bezel* and *no-bezel* smartphone designs depicts future devices. Therefore, the line-of-sight sensors (e.g., front camera) are being tested under the screen for sensing. The authors in [29, 45] study how to recover the images captured by an under-screen camera. In their study, a camera is placed under a 4k transparent OLED display and a pentile OLED display, respectively, to obtain degradation image dataset [45]. Two types of neural networks are proposed to tackle the image degradation [29]. Compared with these studies, we focus on communication with photosensors placed under OLED screen and we have identified the screen's color-pulling effect on color-based VLC signals. We further design SWebCSK modulation to eliminate this effect and thus enable through-screen VLC.

Screen-enabled VLC. Some studies use screens as multi-pixel transmitters to increase the data rate [18, 44]. They exploit standard displays and monitors to achieve screen-to-camera communication. There are also studies using the Liquid Crystal (LC) of LCD screens as reflectors for VLC. PassiveVLC uses a single LC cell to modulate visible light [38]. ChromaLux employs multi-layer LC cells to increase the communication distance and speed [11]. The authors in [26] leverage LCs to enable selective reception of light beams from multiple transmitters. In our system, we use transparent OLED screen instead of an LCD screen. The OLED screen brings opportunities (being transparent) but also challenges (being an interferer) for the realization of through-screen VLC.

9 CONCLUSION

We have studied how to enable through-screen VLC with sensors under the OLED screen. We discovered a color-pulling effect caused by the screen on CSK signals: transmitted CSK symbols are pulled to the detected screen color. We further designed the SWebCSK modulation and proposed a slope-based demodulation and to eliminate the color-pulling effect. We prototyped a system and validated the feasibility of achieving through-screen VLC. We envision that our work could stimulate follow-up studies on through-screen visible light communication and sensing.

ACKNOWLEDGMENTS

The authors would like to thank the anonymous reviewers and the shepherd for their valuable comments and suggestions. This work was supported in part by the Seed Funding of the TU Delft Safety & Security Institute.

REFERENCES

- [1] 2019. IEEE Standard for Local and metropolitan area networks—Part 15.7: Short-Range Optical Wireless Communications. *IEEE Std 802.15.7-2018 (Revision of IEEE Std 802.15.7-2011)* (2019), 1–407. <https://doi.org/10.1109/IEEESTD.2019.8697198>
- [2] Ams. 2018. AS73211. (Feb. 2018). <https://ams.com/as73211>
- [3] Ams. 2019. TCS3701. (July 2019). https://ams.com/documents/20143/36005/Proximity%20Sensors_AN000607_1-00.pdf
- [4] Ams. 2020. TCS34725. (April 2020). https://ams.com/documents/20143/36005/TCS3472_DS000390_3-00.pdf
- [5] Jona Beysens, Qing Wang, Maxim Van den Abeele, and Sofie Pollin. 2021. Blend-VLC: A Cell-free VLC Network Architecture Empowered by Beamspot Blending. In *Proceedings of the IEEE INFOCOM*.
- [6] Rens Bloom, Marco Zuniga, and Chaitra Pai. 2019. Luxlink: Creating a wireless link from ambient light. In *Proceedings of the ACM SenSys*. 166–178.
- [7] Rens Bloom, Marco Zuniga, Qing Wang, and Domenico Giustiniano. 2019. Tweeting with sunlight: Encoding data on mobile objects. In *Proceedings of the IEEE INFOCOM*. 1324–1332.
- [8] CUPC CIE. 1932. Commission internationale de l'éclairage proceedings, 1931. *Cambridge University, Cambridge* (1932).
- [9] 6G Flagship. 2019. Key Drivers and Research Challenges for 6G Ubiquitous Wireless Intelligence. (2019).
- [10] Ander Galisteo, Diego Juara, Qing Wang, and Domenico Giustiniano. 2018. Open-VLC1.2: Achieving higher throughput in low-end visible light communication networks. In *Proceedings of the Annual Conference on Wireless On-demand Network Systems and Services*. 117–120.
- [11] Seyed Keyarash Ghiasi, Marco Zuniga, and Koen Langendoen. 2021. A principled design for passive light communication. In *Proceedings of the ACM MobiCom*. 121–133.
- [12] Harald Haas, Liang Yin, Yunlu Wang, and Cheng Chen. 2016. What is LiFi? *Journal of Lightwave Technology* (2016), 1533–1544.
- [13] Pengfei Hu, Parth H. Pathak, Xiaotao Feng, Hao Fu, and Prasant Mohapatra. 2015. ColorBars: Increasing Data Rate of LED-to-Camera Communication Using Color Shift Keying. In *Proceedings of the ACM CoNEXT*.
- [14] Kingbright. 2014. WP154A4SUREQBFZGC. (Nov. 2014). <https://www.kingbrightusa.com/images/catalog/SPEC/WP154A4SUREQBFZGC.pdf>
- [15] Kingsley Felix. 2021. 39 Smartphones With the Highest Screen to Body Ratio in 2021. (May 2021). <https://thexplorion.com/smartphones-with-the-highest-screen-to-body-ratio/>
- [16] LG. 2021. LG Transparent OLED Signage. (Oct. 2021). <https://www.lg-informationdisplay.com/oled-signage/brand>
- [17] Tianxing Li, Chuankai An, Zhao Tian, Andrew T. Campbell, and Xia Zhou. 2015. Human Sensing Using Visible Light Communication. In *Proceedings of the ACM MobiCom*. 331–344.
- [18] Tianxing Li, Chuankai An, Xinran Xiao, Andrew T. Campbell, and Xia Zhou. 2015. Real-Time Screen-Camera Communication Behind Any Scene. In *Proceedings of the ACM MobiSys*. 197–211.
- [19] Chi Lin, Yongda Yu, Jie Xiong, Yichuan Zhang, Lei Wang, Guowei Wu, and Zhongxuan Luo. 2021. Shrimp: a robust underwater visible light communication system. In *Proceedings of the ACM MobiCom*. 134–146.
- [20] Dong Ma, Guohao Lan, Mahbub Hassan, Wen Hu, Mushfika B. Upama, Ashraf Uddin, and Moustafa Youssef. 2019. SolarGest: Ubiquitous and Battery-Free Gesture Recognition Using Solar Cells. In *Proceedings of the ACM MobiCom*. 1–15.
- [21] Roger Alexander Martínez-Ciro, Francisco Eugenio López-Giraldo, Andrés Felipe Betancur-Perez, and Jose Martín Luna-Rivera. 2019. Design and Implementation of a Multi-Colour Visible Light Communication System Based on a Light-to-Frequency Receiver. *Photonics* (2019).
- [22] MAXVAL. 2020. Featured Technologies: Under Display Sensors. (2020). <https://www.maxval.com/blog/featured-technologies-under-display-sensors/>
- [23] Eric Monteiro and Steve Hranilovic. 2014. Design and Implementation of Color-Shift Keying for Visible Light Communications. *Journal of Lightwave Technology* (2014), 2053–2060.
- [24] LTD OPPO Guangdong Mobile Telecommunications CO. 2020. Electronic equipment and LiFi communication system.
- [25] pureLiFi. 2021. First-ever large-scale deployment of LiFi. (April 2021). <https://purelifi.com/first-ever-large-scale-deployment-of-lifi>
- [26] MD Rahman, Kehinde Adedara, and Ashwin Ashok. 2020. Enabling Multiple Access in Visible Light Communication Using Liquid Crystal Displays: A Proof-of-Concept Study. *Electronics* (2020).
- [27] Sridhar Rajagopal, Richard D. Roberts, and Sang-Kyu Lim. 2012. IEEE 802.15.7 visible light communication: modulation schemes and dimming support. *IEEE Communications Magazine* (2012), 72–82.
- [28] Seth Miller. 2021. Airbus, Latécoère bring LiFi IFE to the business jet market. (May 2021). <https://paxex.aero/airbus-latecoere-lifi-business-jet/>
- [29] Hrishikesh Panikkasseril Sethumadhavan, Densen Puthussery, Melvin Kuriakose, and Jiji Charangatt Victor. 2020. Transform Domain Pyramidal Dilated Convolution Networks for Restoration of Under Display Camera Images. In *European Conference on Computer Vision*. Springer, 364–378.
- [30] Gaurav Sharma and Raja Bala. 2017. *Digital color imaging handbook*. CRC press.
- [31] Sparkfun. 2019. LCD-15079. (Feb. 2019). <https://www.sparkfun.com/products/15079>
- [32] Faisal Tariq, Muhammad R. A. Khandaker, Kai-Kit Wong, Muhammad A. Imran, Mehdi Bennis, and Merouane Debbah. 2020. A Speculative Study on 6G. *IEEE Wireless Communications* (2020), 118–125.
- [33] Purui Wang, Lilei Feng, Guojun Chen, Chenren Xu, Yue Wu, Kenuo Xu, Guobin Shen, Kuntai Du, Gang Huang, and Xuanzhe Liu. 2020. Renovating road signs for infrastructure-to-vehicle networking: A visible light backscatter communication and networking approach. In *Proceedings of the ACM MobiCom*. 1–13.
- [34] Qing Wang, Domenico Giustiniano, and Daniele Puccinelli. 2014. OpenVLC: Software-Defined Visible Light Embedded Networks. In *Proceedings of the ACM MobiCom Workshop on Visible Light Communication Systems*. 15–20.
- [35] Qing Wang, Marco Zuniga, and Domenico Giustiniano. 2016. Passive communication with ambient light. In *Proceedings of the ACM CoNEXT*. 97–104.
- [36] Yue Wu, Purui Wang, Kenuo Xu, Lilei Feng, and Chenren Xu. 2020. Turboboosting visible light backscatter communication. In *Proceedings of the ACM SIGCOMM*. 186–197.
- [37] Jiaojiao Xu, Chen Gong, and Zhengyuan Xu. 2018. Experimental indoor visible light positioning systems with centimeter accuracy based on a commercial smartphone camera. *IEEE Photonics Journal* (2018), 1–17.
- [38] Xieyang Xu, Yang Shen, Junrui Yang, Chenren Xu, Guobin Shen, Guojun Chen, and Yunzhe Ni. 2017. PassiveVLC: Enabling practical visible light backscatter communication for battery-free iot applications. In *Proceedings of the ACM MobiCom*. 180–192.
- [39] Yanbing Yang, Jie Hao, and Jun Luo. 2017. CeilingTalk: Lightweight indoor broadcast through LED-camera communication. *IEEE Transactions on Mobile Computing* (2017), 3308–3319.
- [40] Yanbing Yang, Jie Hao, Jun Luo, and Sinno Jialin Pan. 2017. CeilingSee: Device-free occupancy inference through lighting infrastructure based LED sensing. In *Proceedings of the IEEE PerCom*. 247–256.
- [41] Yanbing Yang and Jun Luo. 2018. Boosting the throughput of LED-camera VLC via composite light emission. In *Proceedings of the IEEE INFOCOM*. 315–323.
- [42] Yanbing Yang, Jun Luo, Chen Chen, Zequn Chen, Wen-De Zhong, and Liangyin Chen. 2021. Pushing the Data Rate of Practical VLC via Combinatorial Light Emission. *IEEE Transactions on Mobile Computing* 20, 5 (2021), 1979–1992.
- [43] Chi Zhang, Josh Tabor, Jialiang Zhang, and Xinyu Zhang. 2015. Extending mobile interaction through near-field visible light sensing. In *Proceedings of the ACM MobiCom*. 345–357.
- [44] Kai Zhang, Yi Zhao, Chenshu Wu, Chaofan Yang, Kehong Huang, Chunyi Peng, Yunhao Liu, and Zheng Yang. 2021. ChromaCode: A Fully Imperceptible Screen-Camera Communication System. *IEEE Transactions on Mobile Computing* (2021), 861–876.
- [45] Yuqian Zhou, Michael Kwan, Kyle Tolentino, Neil Emerton, Sehoon Lim, Tim Large, Lijiang Fu, Zhihong Pan, Baopu Li, Qirui Yang, et al. 2020. UDC 2020 challenge on image restoration of under-display camera: Methods and results. In *European Conference on Computer Vision*. Springer, 337–351.